THE JOURNAL OF BIOLOGICAL CHEMISTRY VOL. 290, NO. 14, pp. 9050–9063, April 3, 2015

Heterodimerization, Altered Subcellular Localization, and Function of Multiple Zinc Transporters in Viable Cells Using Bimolecular Fluorescence Complementation

Received for publication, October 7, 2014, and in revised form, January 21, 2015 Published, JBC Papers in Press, February 5, 2015, DOI 10.1074/jbc.M114.617332

Yarden Golan, Bluma Berman, and Yehuda G. Assaraf[1]

From the Fred Wyszkowski Cancer Research Laboratory, Department of Biology, Technion-Israel Institute of Technology, Haifa 32000, Israel

Background: Upon homodimerization, zinc transporters (ZnTs) mediate zinc efflux and compartmentalization in intracellular organelles.
Results: Bimolecular fluorescence complementation (BiFC) uncovered ZnT heterodimerization, altered subcellular localization, and function.
Conclusion: BiFC uncovers the complex network of ZnT homo-/heterodimers maintaining zinc homeostasis.
Significance: BiFC provides the first *in situ* evidence for the altered subcellular localization and function of ZnT heterodimers in live cells.

Zinc plays a crucial role in numerous key physiological functions. Zinc transporters (ZnTs) mediate zinc efflux and compartmentalization in intracellular organelles; thus, ZnTs play a central role in zinc homeostasis. We have recently shown the *in situ* dimerization and function of multiple normal and mutant ZnTs using bimolecular fluorescence complementation (BiFC). Prompted by these findings, we here uncovered the heterodimerization, altered subcellular localization, and function of multiple ZnTs in live cells using this sensitive BiFC technique. We show that ZnT1, -2, -3, and -4 form stable heterodimers at distinct intracellular compartments, some of which are completely different from their homodimer localization. Specifically, unlike the plasma membrane (PM) localization of ZnT1 homodimers, ZnT1-ZnT3 heterodimers localized at intracellular vesicles. Furthermore, upon heterodimerization with ZnT1, the zinc transporters ZnT2 and ZnT4 surprisingly localized at the PM, as opposed to their vesicular homodimer localization. We further demonstrate the deleterious effect that the G87R-ZnT2 mutation, associated with transient neonatal zinc deficiency, has on ZnT1, ZnT3, and ZnT4 upon heterodimerization. The functionality of the various ZnTs was assessed by the dual BiFC-Zinquin assay. We also undertook a novel transfection competition assay with *ZnT* cDNAs to confirm that the driving force for heterodimer formation is the core structure of ZnTs and not the BiFC tags. These findings uncover a novel network of homo- and heterodimers of ZnTs with distinct subcellular localizations and function, hence highlighting their possible role in zinc homeostasis under physiological and pathological conditions.

Zinc is a trace element required in minute quantities for a multitude of key cellular processes, such as transcription, translation, enzyme activity, cell proliferation, bioenergetics, motility, apoptosis, and autophagy. Therefore, maintenance of zinc homeostasis is crucial for normal growth, differentiation, and development (1, 2). Based on the assessment of the World Health Organization, 17% of the world population are at risk of inadequate zinc intake (3). Zinc deficiency can lead to severe symptoms, such as impaired growth, hypogonadism in males, skin rash, immunological and neurosensory disorders, and cognitive impairment (4). In contrast, high zinc levels may have a toxic effect on multiple cellular functions (5). Hence, cellular, tissue, organ, and whole body zinc homeostasis must be carefully regulated. To meet this crucial requirement, cellular zinc concentration is tightly regulated through zinc transport activity of two distinct zinc transporter families: (*a*) the *SLC30A* gene family, including ZnT1-10, which mediates zinc efflux and compartmentalization in intracellular organelles from the cytosol (6), and (*b*) the *SLC39A* gene family, including ZIP1-14, which mediates zinc uptake from the extracellular milieu into cells (1, 7).

Recently, there has been a growing interest in zinc transporters, particularly in alterations in their function and their implications to human health. Various ZnT[2] mutations were found to be associated with pathological disorders; for example, inactivating mutations in *ZnT2*, a transporter responsible for zinc secretion into breast milk, were found to be associated with transient neonatal zinc deficiency caused by low zinc levels in mother's milk (8–13). Expression of low levels of ZnT3 was associated with learning and memory defects and Alzheimer disease (14), whereas a non-synonymous single nucleotide polymorphism (SNP) in ZnT8 was suggested to increase susceptibility for type 2 diabetes and is associated with young age type 1 diabetes (15, 16). These findings suggest that members of the ZnT family play a key role in maintaining intracellular zinc homeostasis and human health.

[1] To whom correspondence should be addressed. Tel.: 972-4-8294211; Fax: 972-4-8295670; E-mail: assaraf@tx.technion.ac.il.

[2] The abbreviations used are: ZnT, zinc transporter; BiFC, bimolecular fluorescence complementation; TPEN, *N*,*N*,*N*′,*N*′-tetrakis(2-pyridylmethyl)ethane-1,2-diamine; WGA, wheat germ agglutinin; ER, endoplasmic reticulum; PM, plasma membrane.

Based on the crystal structure of YiiP, a ZnT homologue from *Escherichia coli*, the ZnT family was predicted to have six transmembrane domains with the C and N termini located in the cytoplasm (17). Moreover, excluding ZnT6, all ZnTs harbor two highly conserved hydrophilic residues located in transmembrane domains II and V, which are involved in zinc binding (18, 19). The C-terminal domains of YiiP have a major impact on its dimerization, which is stabilized by four zinc ions mediating the formation of a tight interface between the interacting monomers, as revealed by x-ray crystallography (17). In contrast, the transmembrane domains were suggested to form conformational changes that are relevant to the alternating access mechanism for zinc transport (17).

Previous studies have suggested that, like YiiP, members of the ZnT family also form homodimers; for instance, ZnT3 was shown to form homodimers via covalent dityrosine bonds (20). Furthermore, using epitope tagging and co-immunoprecipitation, ZnT5 and ZnT6 were shown to form a stable heterodimer (21), although more sensitive tools were needed to corroborate ZnT dimerization and to follow the subcellular localization of these dimers in live cells. In this respect, we recently applied the bimolecular fluorescence complementation (BiFC) technique in order to provide direct visual evidence for the *in situ* dimerization of wild type (WT) and mutant ZnTs in live cells at their established intracellular organelles (22). The BiFC technique, which was originally devised to visualize specific protein-protein interactions in live cells (23), is based on the principle of tagging two proteins with two non-fluorescent halves of a fluorescent protein, such as yellow fluorescence protein (YFP). Once the two target proteins undergo a close physical interaction (less than 15 nm), this facilitates the non-fluorescent fragments of YFP to associate and refold, thereby leading to the resumption of YFP fluorescence (24). This sensitive bioassay enabled us to detect high fluorescence levels, which were indicative of homodimer formation of various ZnTs, including ZnT1–4 and ZnT7 (22). Furthermore, this BiFC assay allowed us to pinpoint the precise subcellular localization of ZnT5 and ZnT6 heterodimers in live cells (22). In order to explore the *in situ* functionality of WT and mutant ZnT2 dimers, we used the viable fluorescent zinc probe, Zinquin, along with the BiFC assay. Hence, the dual BiFC-Zinquin assay provided the first *in situ* evidence for the homodimerization and function of WT and mutant ZnT2 in live cells. Prompted by these findings, we here aimed at determining whether or not multiple ZnTs form heterodimers and further examined their subcellular localization and zinc compartmentalization in cells co-expressing two distinct ZnTs. We show for the first time the heterodimerization of multiple ZnTs, their altered subcellular localization, and intracellular zinc compartmentalization. These novel findings bear important implications for the molecular mechanisms underlying intracellular zinc homeostasis under physiological and pathological conditions.

MATERIALS AND METHODS

Chemicals and Reagents—The DNA dyes DAPI and Hoechst 33342 as well as the cell-permeant zinc chelator *N,N,N′,N′*-tetrakis(2-pyridylmethyl)ethane-1,2-diamine (TPEN) were purchased from Sigma-Aldrich. The fluorescent zinc probe Zinquin ethyl ester was purchased from Biotium (Hayward, CA), whereas zinc sulfate was obtained from Merck. The fluorescent conjugate wheat germ agglutinin (WGA) Texas Red®-X conjugate, MitoTracker Red CMXRos, and LysoTracker Red DND-99 were obtained from Invitrogen.

Generation of cDNA Constructs—ZnT BiFC constructs were generated as described previously (22). In brief, the coding regions of the long isoforms of ZnT1–7 were amplified by PCR from expression plasmids harboring these cDNAs (kindly provided by Prof. T. Kambe, Kyoto University, Kyoto, Japan). The purified PCR products were then digested with the appropriate restriction enzymes and cloned into the BiFC constructs as described previously (22). Ligation products were transformed into heat shock-competent *E. coli* DH5α, and positive colonies were selected using PCR. The fidelity of the insert and the tags were confirmed by direct DNA sequencing (Technion, Rappaport School of Medicine, DNA Sequencing Facility, Haifa, Israel). The G87R mutation was introduced into the *ZnT2* expression plasmids using *Pfu* Turbo DNA polymerase (QuikChange kit, Stratagene, La Jolla, CA) and the following primers: forward primer, 5′-CTGCCTGTTGTTCATGATC-CGAGAAGTCGTTGAGATC-3′; reverse primer, 5′-GATCT-CAACGACTTCTCGGATCATGAACAACAGGCAG-3′.
ZnT3-Myc was cloned from a pA-Ecogtp plasmid (kindly provided by Prof. T. Kambe, Kyoto University). *ZnT3-Myc* was digested with *EcoRI* and *NotI* and cloned into a pcDNA4/TO vector at a vector/insert ratio of 1:4. The ligation (DNA Ligation Kit, Taraka Bio Inc., Shiga, Japan) was performed for 5 min at room temperature, and ligation products were processed as described above. *ZnT5-Myc* plasmid was kindly provided by Prof. E. C. Dell'Angelica (UCLA, Los Angeles, CA). The *THTR1-Myc* expression plasmid was kindly provided by Prof. A. Aronheim (Technion, Haifa, Israel).

Cell Culture and Transient Transfection—MCF-7 breast cancer cells were grown as described previously (22). Cells were seeded (5×10^4 cells/well) in 24-well glass bottom plates (In Vitro Scientific, Sunnyvale, CA) for fluorescence microscopy, or in 6-well or 12-well plates (2×10^5 cells/well of 6-well plates and 10^5 cells/well of 12-well plates; Nunc A/S, Roskilde, Denmark) for flow cytometry and Western blot analyses. Following an overnight incubation at 37 °C, cells were transiently transfected (3 μg of plasmid DNA/well of 6-well plates; 1 μg plasmid DNA/well of 24-well, plates or 2 μg plasmid DNA/well of 12-well plates) using jetPEI (Polyplus Transfection, SA, Illkirch, France) at a DNA/transfection reagent ratio of 1:2, according to the instructions of the manufacturer for an incubation time of up to 24 h.

Fluorescence Microscopy—24 h after transfection, the growth medium was removed, and monolayer cells were washed with PBS and then incubated in PBS containing 1 mM $MgCl_2$, 1 mM $CaCl_2$, and 10 mM D-glucose at pH 7.4. Hoechst 33342 (2 μg/ml) was used for nuclear DNA staining. LysoTracker Red (100 nM, for 1 h), MitoTracker Red (100 nM, for 1 h), and WGA (5 μg/ml for 10 min) were used as organelle markers. Live cells were imaged using an inverted confocal microscope (Zeiss LSM 710) at a magnification of ×63 under immersion oil. Immunofluorescence imaging was performed using a Zeiss Axiovert 200

Cell Observer inverted microscope at a magnification of ×63 under immersion oil.

Flow Cytometry—Transiently transfected MCF-7 cells were analyzed by flow cytometry for both the percentage of YFP-positive cells and the YFP fluorescence levels. Cells were washed three times with PBS, detached by trypsinization, and harvested in sterile Eppendorf tubes. Cells were centrifuged at 660 × *g* for 5 min, resuspended in 0.5 ml of PBS, and transferred into flow cytometer test tubes at a cell density of ~2.4 × 10^6 cells/ml. 10,000 cells were analyzed for each transfection.

Assessment of ZnT Heterodimerization in BiFC Transfectants Using Western Blot Analysis—MCF-7 cells were transiently co-transfected with an equal amount of the designated plasmids (1.5 μg of DNA of each construct). Membrane proteins were isolated on ice using an extraction buffer containing 50 mM Tris-HCl, pH 7.5, 50 mM β-mercaptoethanol, 0.5% Triton X-100, 1 mM EDTA, 1 mM EGTA, and a protease inhibitor mixture (Roche Applied Science). Proteins (40 μg) were resolved by electrophoresis on 10% polyacrylamide gels containing SDS, electroblotted onto Protran BA83 cellulose nitrate membranes (Schleicher & Schuell), blocked with Tris-buffered saline (TBS)-milk (TBS contained 10 mM Tris-Cl, 150 mM NaCl, 0.5% Tween 20, and 20% milk (1% fat) at pH 8), and reacted with mouse anti-ZnT2 or anti-ZnT4 monoclonal antibodies (at 1:2000 dilution, for 1 h at room temperature; generously provided by Prof. T. Kambe (Kyoto University)). Blots were then washed three times with TBS for 10 min each at room temperature and incubated with horseradish peroxidase-conjugated goat anti-mouse IgG (1:20,000 dilution; Jackson Immunoresearch Laboratories, West Grove, PA) for 1 h at room temperature. After three 10-min washes in TBS at room temperature, enhanced chemiluminescence detection was performed according to the manufacturer's instructions (Biological Industries, Beth-Haemek, Israel). ER stress was assessed using a goat-anti-GRP78 antibody (1:625 dilution; Santa Cruz Biotechnology, Inc., Dallas, TX) and detected with horseradish peroxidase-conjugated donkey anti-goat IgG (1:20,000 dilution; Jackson Immunoresearch Laboratories).

Analysis of Vesicular Zinc Accumulation in Viable Cells—In order to assess vesicular zinc accumulation in transfected cells, we used the viable zinc probe, Zinquin ethyl ester, as described previously (22). 21 h after transfection, cells were incubated in growth medium containing 75 μM $ZnSO_4$ for 2 h. Cells were then rinsed twice with PBS and incubated in growth medium containing 40 μM Zinquin ethyl ester for 1 h at 37 °C. Finally, cells were washed three times with PBS, suspended in 0.5 ml of PBS, and analyzed by flow cytometry or imaged using an inverted confocal microscope as described above.

Chelation of Cellular Zinc Using TPEN—In order to verify that Zinquin staining is dependent on cellular zinc accumulation, we used increasing concentrations (0–120 μM) of the cell-permeant zinc chelator TPEN. Cells were transfected with YFP empty vector or ZnT2-YC-YN constructs and were incubated with Zinquin as described above. Increasing concentrations of TPEN were added for 1 h in the presence of Zinquin, and cells were then washed three times and analyzed or incubated for another 1 h in growth medium (a total incubation time of 2 h for TPEN). Cells were analyzed using flow cytometry.

Subcellular Co-localization of ZnT2-HA with ZnT3-Myc—Expression plasmids harboring *ZnT2-HA* and *ZnT3-Myc* were transiently transfected into MCF-7 cells as described above. Cells plated onto glass coverslips were fixed with 4% formaldehyde in PBS for 30 min and permeabilized with 0.1% Triton X-100 in PBS for 5 min. Nonspecific binding was blocked by 1-h incubation with TBS containing 20% skim milk (1% fat). Cells were washed twice with PBS for 5 min, and detection of ZnT2-HA was performed by incubation with rabbit anti-HA antibody (4 μg/ml; Abcam) for 1 h at room temperature, whereas detection of ZnT3-Myc was undertaken by incubation with mouse anti-Myc (5 μg/ml; Abcam) for 1 h. Cells were then washed twice with PBS each for 5 min and incubated for 1 h at room temperature, protected from light with rhodamine red-conjugated anti-rabbit IgG (1:100; Jackson ImmunoResearch) and Cy2-conjugated anti-mouse antibody (1:100; Jackson ImmunoResearch) as the secondary antibodies. Nuclei were stained with DAPI (0.5 μg/ml).

Competition Assay with Non-BiFC-tagged ZnT and THTR-1 cDNAs—MCF-7 cells were co-transfected with equal amounts of expression plasmids harboring YC-tagged ZnT or YN-tagged ZnT (0.5 μg of plasmid DNA of each YC- or YN-tagged ZnT) along with increasing amounts of the competitor plasmid containing the cDNA of the non-YC-YN-tagged ZnT (0–2 μg of plasmid DNA plasmid) harboring an epitope tag (HA for ZnT2 and Myc for both ZnT3, ZnT5 and THTR1 (*SLC19A2*)). The total amount of plasmid DNA (3 μg) was supplemented with an empty vector. 24 h after transfection, YFP fluorescence was determined using flow cytometry. We determined the maximal YFP intensity for each pair of transporters, when no competitor ZnT cDNA (tagged with HA or Myc) was added (where 100% of YFP fluorescence is the initial fluorescence). Next, we calculated the decrease or increase in the percentage of YFP fluorescence compared with the fluorescence intensity observed in the absence of the competitor plasmid.

Statistical Analysis—Results are presented as means ± S.D. Statistical comparisons were performed using Student's *t* test (GraphPad Prism, GraphPad Software, La Jolla, CA), and a significant difference was demonstrated when p was <0.05. Results from at least three independent experiments are shown.

RESULTS

The BiFC Technique Uncovers a Remarkable Interaction between Multiple ZnTs—Our previous BiFC study demonstrated a marked homodimerization between ZnT1–4 and ZnT7 monomers as well as the formation of ZnT5-ZnT6 heterodimers at their established intracellular compartments (22). Herein we applied the BiFC assay to explore the possible heterodimerization of various ZnTs. MCF-7 cells were co-transfected with non-fluorescent BiFC-tagged ZnTs, including ZnT1–4 and ZnT6; specifically, these ZnTs were C-terminally tagged with YC (*i.e.* ZnT-YC) along with ZnT2 or ZnT4, which were tagged with YN (ZnT-YN**;** Fig. 1*A*). Flow cytometric analysis enabled us to determine two parameters that reflect specific dimerization of the various ZnTs: (*a*) the percentage of transfected cells displaying YFP fluorescence as a result of YC-YN refolding, which was above the autofluorescence level obtained with untransfected cells, and (*b*) mean fluorescence of

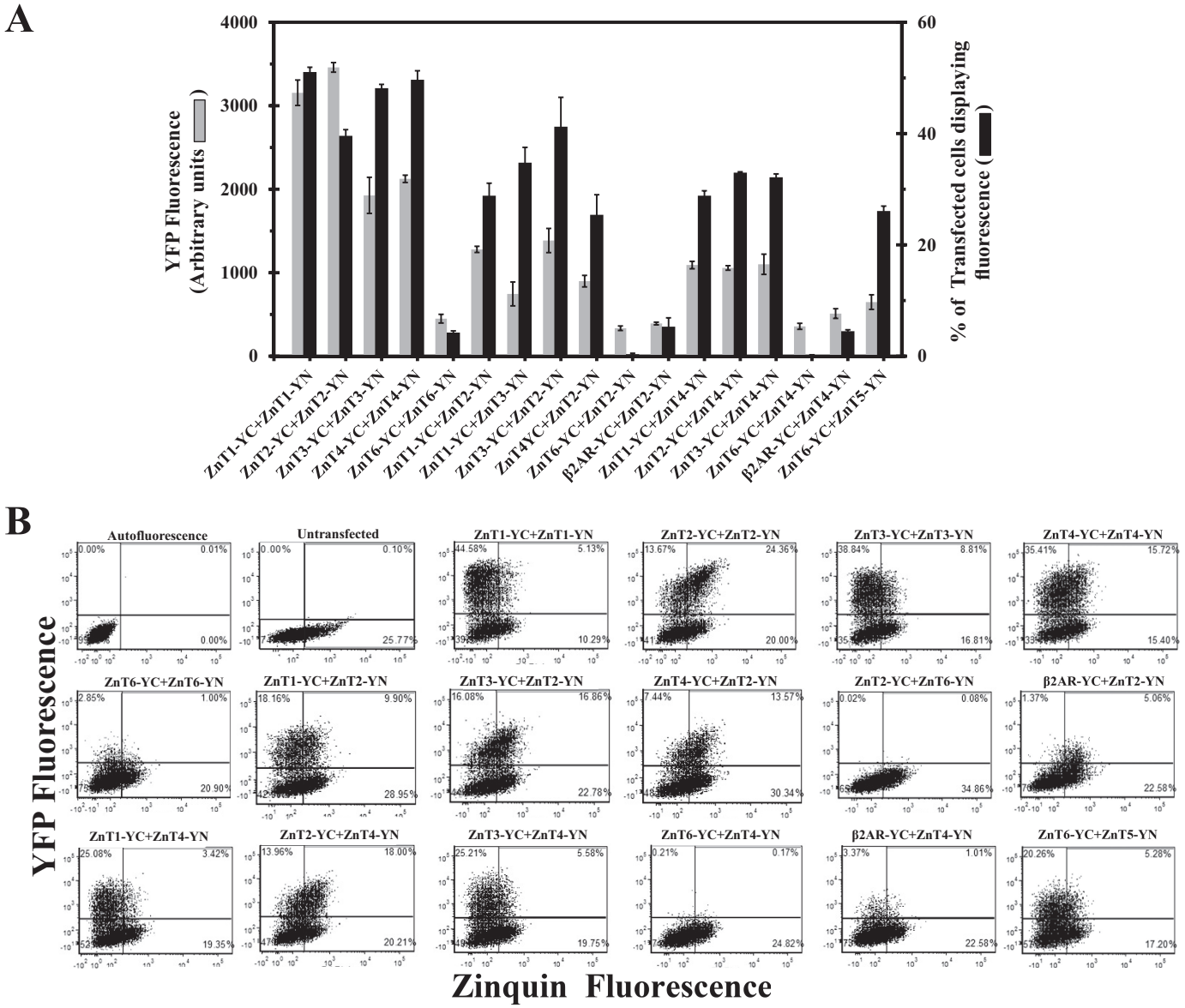

FIGURE 1. **The BiFC assay reveals that ZnT2 and ZnT4 form heterodimers with ZnT1–4 but not with ZnT6.** *A*, MCF-7 cells were transiently co-transfected with ZnT plasmid pairs as described below. The percentage of transfected cells displaying YFP fluorescence (*black bars*) and the mean YFP fluorescence intensity (*gray bars*) were determined using flow cytometry and represent the fraction of ZnT-YC-YN fluorescent cells. The negative controls consisted of co-transfection of ZnT2-YC and β2AR-YN as well as ZnT4-YC and β2AR-YN. All *p* values ($p < 0.05$) denote statistically significant differences when compared with the negative control of ZnT2-YC + β2AR-YN, except for the values obtained with the percentage of transfected cells upon co-transfection of ZnT6-YC-YN and ZnT4-YC + β2AR-YN. *Error bars*, S.D. *B*, flow cytometric dot plot analysis from a representative experiment. MCF-7 cells were transiently co-transfected with the constructs described *above* the dot plots. The *y* axis represents the YFP fluorescence levels, whereas the *x* axis represents Zinquin fluorescence levels. Each *dot* represents a single cell. Quadrants were determined using the background autofluorescence dot plot. *Top quadrants* represent cells that display a YFP fluorescence that was above the background autofluorescence level (transfected cells). *Right quadrants* represent cells that display Zinquin fluorescence. The *top right quadrant* represents cells that exhibited both YFP and Zinquin fluorescence.

transfectant cells displaying YFP fluorescence, which represents the strength of the dimerization culminating in a metastable YC-YN interaction. As we showed previously (22), cells co-transfected with *ZnT1-YC-YN*, *ZnT2-YC-YN*, *ZnT3-YC-YN*, or *ZnT4-YC-YN* displayed high levels of YFP fluorescence as a result of homodimerization. In contrast, co-transfection of MCF-7 cells with *ZnT6-YC-YN* resulted in very low YFP fluorescence levels in a very small fraction of cells, indicating the lack of substantial ZnT6 homodimerization (Fig. 1*A*, *left part* of *histogram*). We next co-transfected MCF-7 cells with *ZnT2-YN* and *ZnT1–4-YC* to determine whether or not ZnT2 forms heterodimers with other ZnTs. MCF-7 cells co-transfected with *ZnT2-YN*, together with either *ZnT1-YC*, *ZnT3-YC*, or *ZnT4-YC*, exhibited moderate fluorescence levels when compared with their homodimers; the fluorescence levels of these heterodimers were significantly higher than the nonspecific background fluorescence obtained upon co-expression of ZnT2-YN and β2AR-YC (Fig. 1*A*). In contrast, co-transfection of *ZnT2-YN* and *ZnT6-YC* revealed very low fluorescence levels, even lower than for ZnT6 homodimers, indicating the lack of a significant formation of ZnT2-ZnT6 heterodimers and/or their possible fast degradation. Moreover, cells co-transfected with *ZnT4-YN* along with either *ZnT1-YC*, *ZnT2-YC*, or *ZnT3-YC* showed moderate fluorescence levels compared with their

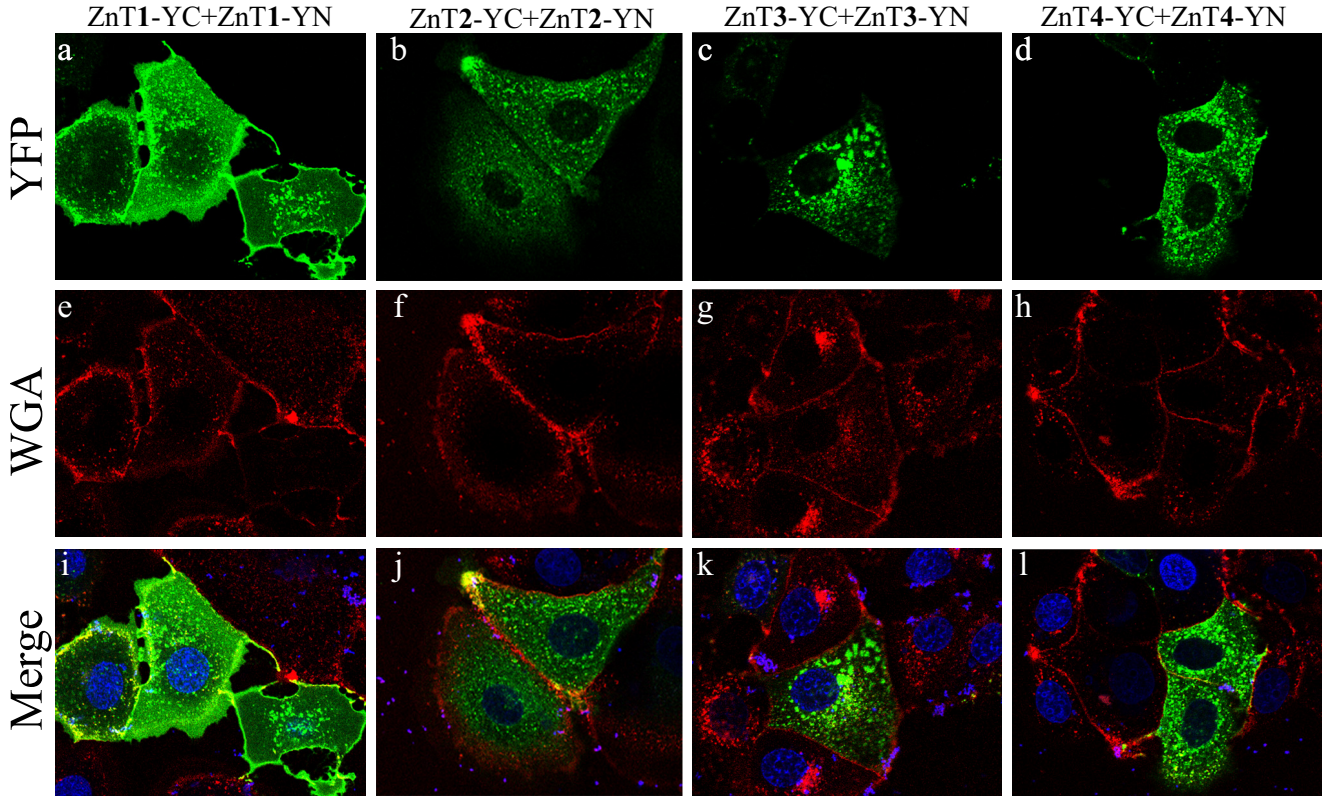

FIGURE 2. **Subcellular localization of ZnT1–4 homodimers.** MCF-7 cells were transiently co-transfected with the constructs described *above* the *panels*. The *green* YFP fluorescence signal (YC-YN fluorescence) indicates homodimer formation. The *red* fluorescence signal indicates WGA Texas Red staining. Hoechst 33342 (*blue* fluorescence) was used to stain nuclei. Live MCF-7 cells were examined using confocal fluorescence microscopy (LSM 710). A magnification of ×63 under immersion oil was used.

homodimers but were significantly higher when compared with the very small fraction of the background fluorescent cells (4%) obtained with the *β2AR-YC* and *ZnT4-YN* co-transfection, which served as a negative control (Fig. 1*A*). Moreover, co-transfection of *ZnT4-YN* along with *ZnT6-YC* resulted in very low fluorescence levels. In contrast, co-transfection of *ZnT5-YN* and *ZnT6-YC* resulted in substantial fluorescence levels in a relatively large fraction of cells (27%; Fig. 1*A*); the latter ZnT5-ZnT6 heterodimers served as a positive control because they were previously shown to function as heterodimers in the early secretory pathway (21). However, the mean fluorescence level of ZnT5-ZnT6 heterodimers was lower than other heterodimers, perhaps reflecting lower expression levels as well as a distinct intracellular localization at the *trans*-Golgi network, as opposed to other ZnTs harboring PM (ZnT1) and intracellular vesicle localization (ZnT2, -3, and -4). To assess the functionality of these various ZnT dimerizations, flow cytometry dot plots were undertaken that compared YFP fluorescence *versus* Zinquin fluorescence (Fig. 1*B*). This two-dimensional quadrant analysis highlighted the differences in the functionality of the various ZnT pairs studied here (Fig. 1*B*). The percentage of YFP and Zinquin fluorescent cells in the *top right quadrant* for each ZnT dimer was determined when compared with the background autofluorescence dot plot. To calculate Zinquin accumulation (elaborated in Fig. 7*A*), we divided the percentage of cells that displayed YFP and Zinquin fluorescence (*top right quadrants*) by the percentage of cells displaying YFP fluorescence (*top quadrants*). Cells expressing ZnT1–4 homodimers showed a larger fraction of cells in the *top quadrants* (*i.e.* both larger fraction of transfected cells and higher fluorescence levels), when compared with various heterodimers of ZnT1–4. However, cells expressing heterodimers of ZnT1–4 showed a larger fraction of cells in the *top quadrants* when compared with the negative controls of ZnT2 or ZnT4 that were co-transfected with *β2AR-YC*. Importantly, cells co-transfected with *ZnT2-YC-YN* showed the largest fraction of cells in the top right quadrant, indicating a high Zinquin accumulation in these cells. Heterodimers of ZnT2-ZnT4 and ZnT2-ZnT3 preserved high levels of Zinquin accumulation as indicated by the relatively large fraction of cells that were in the *top right quadrants* (Fig. 1*B*). These results demonstrate the formation of heterodimers of ZnT1–4, as indicated by the moderate levels of YFP fluorescence levels when compared with the negative control. Moreover, this two-dimensional dot plot analysis of YFP fluorescence *versus* Zinquin fluorescence reveals the ability of cells containing ZnT2-ZnT3 and ZnT2-ZnT4 heterodimers to accumulate intravesicular Zinquin (Fig. 1*B*), hence providing an important indication as to the functionality of certain heterodimers in zinc transport.

The BiFC technique enabled the *in situ* visualization of the subcellular localization of the various ZnT heterodimers in live cells. In the current study, we employed the viable PM marker WGA-Texas Red, to show that ZnT1-YC-YN homodimers localized at the PM and in some perinuclear compartments (Fig. 2, *a*, *e*, and *i*). In contrast, ZnT2, ZnT3, and ZnT4 homodimers localized predominantly in intracellular vesicles

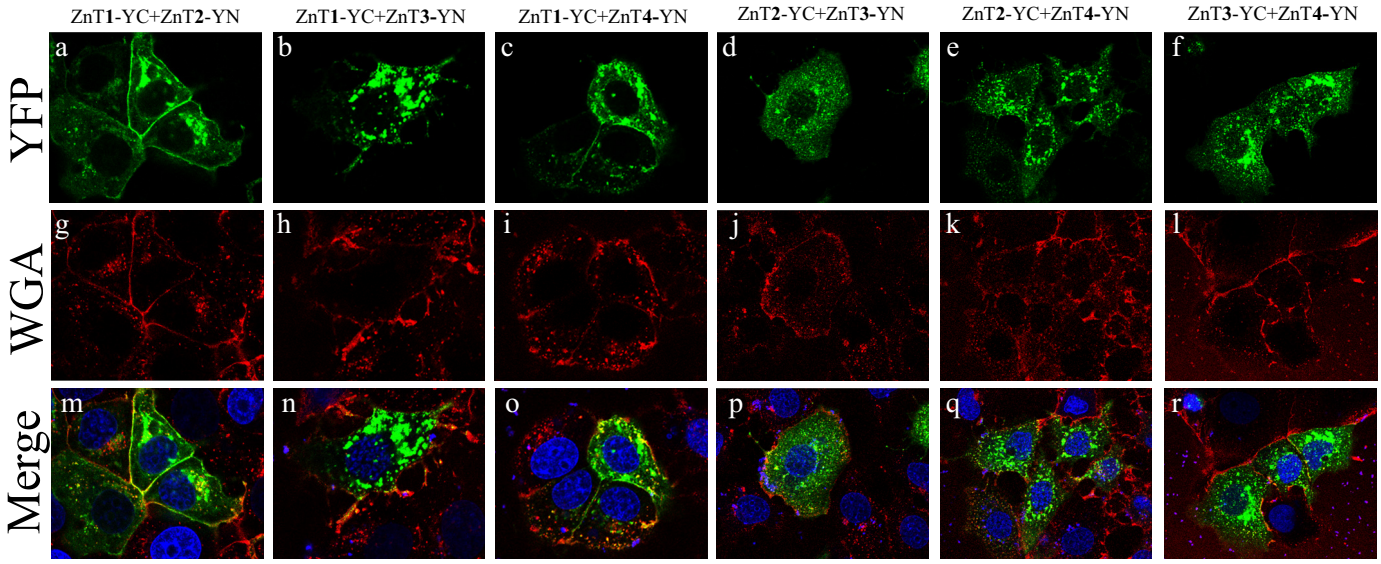

FIGURE 3. **Subcellular localization of ZnT1–4 heterodimers.** MCF-7 cells were transiently co-transfected with the constructs described *above* the *panels*. The *green* YFP fluorescence signal (YC-YN fluorescence) indicates heterodimer formation. The *red* fluorescence signal indicates WGA Texas Red staining. Hoechst 33342 (*blue* fluorescence) was used to stain nuclei. Live MCF-7 cells were examined using confocal fluorescence microscopy (LSM 710). A magnification of ×63 under immersion oil was used.

(Fig. 2, *j–l*), such as endosomal/secretory compartments, and did not co-localize with this PM marker but only with intracellular vesicles of WGA, which were presumably internalized from the PM via endocytosis. Surprisingly, co-transfection of *ZnT1-YC* and *ZnT2-YN* revealed a moderate to strong YFP fluorescence of ZnT1-ZnT2 heterodimers that predominantly localized at the PM, as indicated by co-localization with WGA, in the vast majority of co-transfectant cells, albeit some localization was also apparent at intracellular vesicles and at the perinuclear compartment (Fig. 3, *a*, *g*, and *m*). Hence, ZnT1-ZnT2 heterodimers acquire the PM localization of ZnT1 homodimers rather than the vesicular localization of ZnT2 homodimers. Interestingly, ZnT1-YC-ZnT3-YN heterodimers that showed moderate to high fluorescence levels localized solely at intracellular vesicles and hence did not reach the PM, as observed here for ZnT1-ZnT2 heterodimers (Fig. 3, *b*, *h*, and *n*). Remarkably, ZnT1-YC-ZnT4-YN heterodimers were also found to localize at the PM in most of the co-transfectant cells displaying YFP fluorescence, in addition to some perinuclear and intracellular vesicle localization (Fig. 3, *c*, *i*, and *o*). In contrast, ZnT2-YC-ZnT3-YN and ZnT2-YC-ZnT4-YN heterodimers localized exclusively at intracellular vesicles (Fig. 3, *d*, *j*, and *p* and *e*, *k*, and *q*, respectively). As expected, ZnT3-YC-ZnT4-YN heterodimers localized at intracellular vesicles, hence retaining the native localization of their homodimers (Fig. 3, *f*, *l*, and *r*). We next explored the possibility that ZnT1 homodimers, which display PM localization, and ZnT2 homodimers, which represent a dominant localization at intracellular vesicles, co-localized with the lysosomal marker LysoTracker Red or with the mitochondrial marker MitoTracker Red in live cells (Fig. 4). As expected, no co-localization of ZnT1 homodimers with either LysoTracker or MitoTracker was found (Fig. 4, *A* and *B*, *a–c*), further establishing the dominant PM localization of ZnT1. In agreement with previous reports (25–27), we found partial co-localization of ZnT2 with LysoTracker, albeit transfected MCF-7 cells did not display high levels of LysoTracker staining (Fig. 4*A*, *d–f*). No co-localization was found with ZnT2 and MitoTracker (Fig. 4*B*, *d–f*). These results suggest that in MCF-7 transfectants, ZnT2 is localized at intracellular vesicles that are probably endo-/exocytotic vesicles or zincosomes (1). This localization is consistent with the role of ZnT2 in zinc secretion into breast milk in mammary gland epithelial cells. In contrast to previous papers that established the localization of ZnT2 (22, 25, 26, 28, 29) in MCF-7 cells, ZnT2 did not co-localize at mitochondria and was only partially localized at acidic vesicles like lysosomes. Collectively, these results provide the first *in situ* evidence for the formation of heterodimers composed of ZnT1 and ZnT2–4, ZnT2 and ZnT3–4, as well as ZnT3 and ZnT4. Furthermore, these findings suggest a dominant localization effect of ZnT1 over ZnT2 and over ZnT4 upon heterodimerization because these heterodimers predominantly resided in the PM. In contrast, upon heterodimerization, ZnT3 appears to exert a dominant effect over ZnT1, resulting in an exclusive vesicular localization of ZnT1-ZnT3 heterodimers.

Corroboration of Heterodimerization by Western Blot Analysis Using ZnT2- and ZnT4-specific Antibodies—Previously, we have shown that ZnT2-YC-YN homodimers were detectable upon electrophoresis on SDS gels under denaturing conditions (22). These results suggested that ZnT2-YC and ZnT2-YN form metastable (*i.e.* irreversible) homodimers, presumably due to the refolding into a fully fluorescent YFP protein (22) and the formation of covalent bonds (30). Prompted by these findings, we further explored here ZnT heterodimerization by Western blot analysis (Fig. 5, *A* and *B*). Furthermore, because both flow cytometric analysis and fluorescence microscopy are based on YFP fluorescence, Western blot analysis can detect physical interactions between different ZnTs and quantify the actual ZnT protein levels. Consistent with the results presented in Fig. 1, Western blot analysis performed with an antibody against ZnT2 revealed that the strongest interaction of ZnT2-YN was with ZnT2-YC in the homodimer form (Fig. 5*A*).

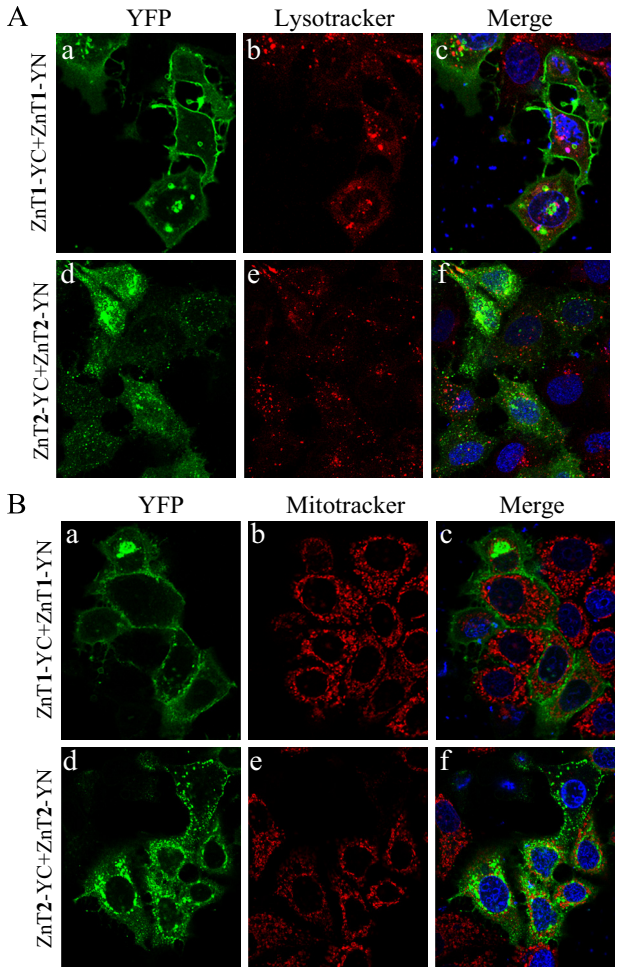

FIGURE 4. **Identification of lysosomal or mitochondrial localization of ZnT1 and ZnT2 homodimers.** MCF-7 cells were transiently co-transfected with the constructs described on the *left side* of the *panels*. The *green* YFP fluorescence signal (YC-YN fluorescence) indicates homodimer formation. Hoechst 33342 (*blue* fluorescence) was used to stain nuclei. *A*, the *red* fluorescence signal indicates LysoTracker red staining. *B*, the *red* fluorescence signal indicates MitoTracker red staining. Live MCF-7 cells were examined using confocal fluorescence microscopy (LSM 710). A magnification of ×63 under immersion oil was used.

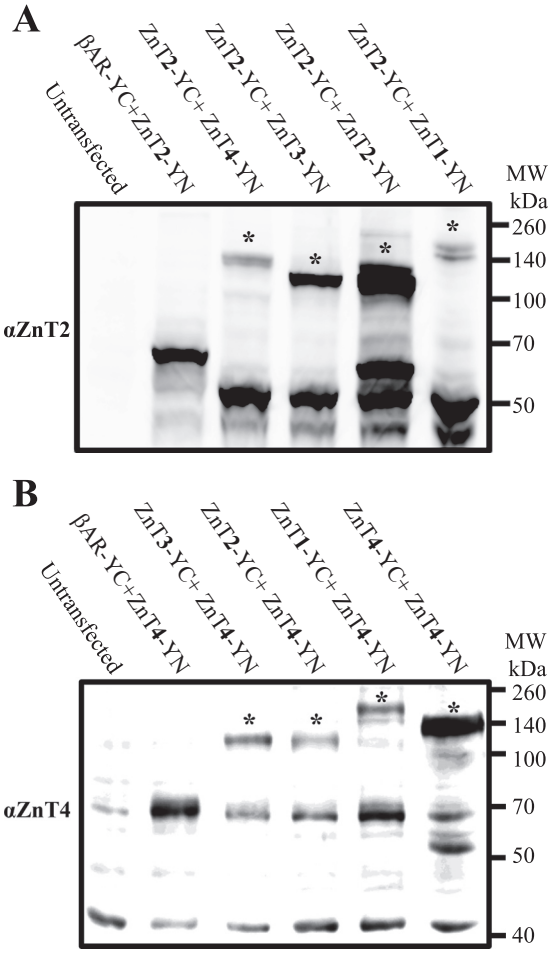

FIGURE 5. **Western blot analysis using ZnT2- and ZnT4-specific antibodies corroborates heterodimer formation.** Shown is Western blot analysis of ZnT2 and ZnT4 heterodimers in various ZnT co-transfectant pairs. MCF-7 cells were transiently co-transfected with the constructs described *above*. Western blot analysis was performed after SDS-PAGE under denaturing conditions using an anti-ZnT2 antibody (*A*) or an anti-ZnT4 antibody (*B*). The *asterisks* show the higher molecular weight bands that represent the putative complex of ZnT2-YN and ZnT1–4-YC with a molecular mass of ~110 kDa or more, depending on the size of the specific ZnT.

ZnT2 homodimerization (Fig. 5*A*) was more stable than the various heterodimers, including the following pairs: ZnT2 and ZnT1, ZnT2 and ZnT3, as well as ZnT2 and ZnT4. Similarly, using an antibody to ZnT4, we found that ZnT4 homodimerization was more stable than various heterodimers including the following pairs: ZnT4 and ZnT1, ZnT4 and ZnT2, as well as ZnT4 and ZnT3 (Fig. 5*B*). We also demonstrated the formation of heterodimers of ZnT2-YC and ZnT4-YN, based on the identification of a higher molecular mass band of ~140 kDa, using both anti-ZnT2 and anti-ZnT4 antibodies (Fig. 5, *A* and *B*). The homodimer bands were more intense when compared with heterodimer bands, hence indicating a stronger interaction of the homodimers than of the heterodimers (Fig. 5, *A* and *B*). The observed differences in the apparent molecular masses of the different dimer bands are consistent with the predicted molecular mass of the various ZnTs based on their amino acid sequence. As expected, no dimer bands were observed upon co-transfection of *ZnT2-YN* with *β2AR-YC*, indicating that there was no specific interaction between ZnT2-YN and β2AR-YC (Fig. 5, *A* and *B*). These results suggest that various ZnTs may form heterodimers and further indicate that the interactions between ZnT2 and ZnT1,3,4 are intense and specific, whereas the negative control ZnT2 and β2AR failed to form dimers. Moreover, these results suggest that there was no protein degradation of ZnT2-YN due to nonspecific interaction with β2AR because the levels of ZnT2-YN bands remained constant.

Fluorescence Microscopy Reveals That Transient Co-transfection of ZnT2-HA and ZnT3-Myc Results in Co-localization at Their Original Intracellular Vesicular Sites—We focused on the interaction between ZnT2 and ZnT3 as well as that of ZnT2 and ZnT4 because they displayed a strong interaction in the BiFC assay (Figs. 1 and 5), and they localized at their original intracellular vesicular sites. ZnT2 and ZnT4 were previously shown to co-localize at the same intracellular compartment and to function together in loading zinc into lysosomes (26). To determine the localization of ZnT2 and ZnT3, MCF-7 cells were transiently co-transfected with plasmids harboring epitope-tagged *ZnT2-HA* and *ZnT3-Myc*. Immunofluores-

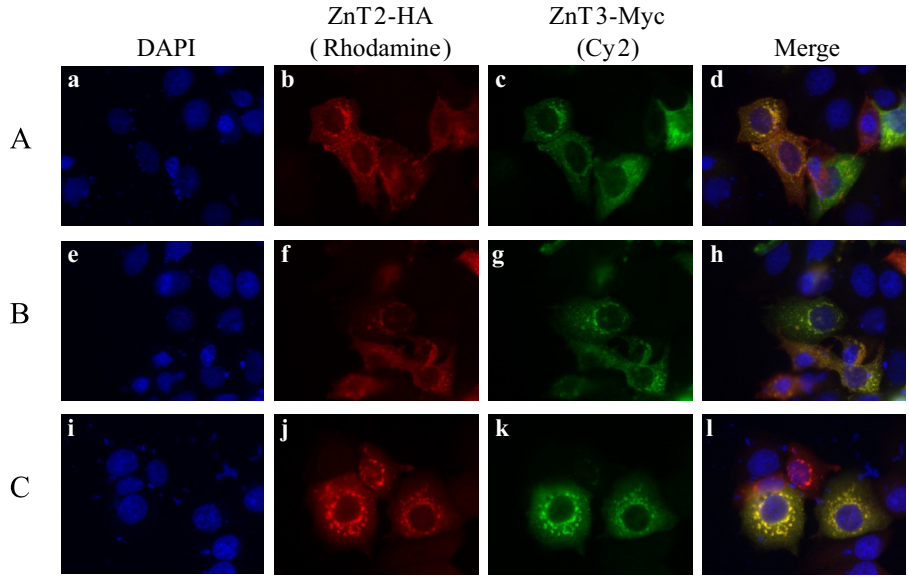

FIGURE 6. **Subcellular co-localization of ZnT2-HA and ZnT3-Myc.** Localization of HA-tagged ZnT2 (*b*, *f*, and *j*) and Myc-tagged ZnT3 (*c*, *g*, and *k*) in co-transfectants of MCF-7 was examined using Cell Observer fluorescence microscopy. Detection of ZnT2 was performed using a rabbit anti-HA antibody and a rhodamine red anti-rabbit as secondary antibody (*red* fluorescence; *b*, *f*, and *j*), whereas detection of ZnT3-Myc was performed using a mouse anti-Myc antibody and Cy2-anti-mouse as a secondary antibody (*green* fluorescence; *c*, *g*, and *k*). *Merged images* illustrate vesicular co-localization of ZnT2 and ZnT3 (*d*, *h*, and *l*). Nuclei were stained with DAPI (*blue* fluorescence; *a*, *e*, and *i*). *A–C*, three independent transfection experiments. A magnification of ×63 under immersion oil was used.

cence analysis was performed using anti-Myc and anti-HA as primary antibodies, followed by anti-mouse-conjugated Cy2 and anti-rabbit-conjugated rhodamine as secondary antibodies, respectively (Fig. 6). ZnT2-HA and ZnT3-Myc co-localized at the same intracellular vesicles, hence indicating that they are both targeted to the same subcellular compartments.

Exploration of the Function of ZnT2-ZnT4 Heterodimers Using the Dual BiFC-Zinquin Assay—Zinc accumulation was assessed using the viable cell-permeant fluorescent zinc probe Zinquin ethyl ester, the fluorescence of which is enhanced upon zinc binding (22). As such, accumulation of higher zinc concentrations in intracellular compartments, such as vesicles mediated by ZnT2 for example, results in higher Zinquin fluorescence levels in a higher fraction of cells, as we have shown previously (22). In this assay, we determined the percentage of Zinquin accumulation as the fraction of cells displaying YFP fluorescence together with Zinquin fluorescence divided by the fraction of cells exhibiting only YFP fluorescence. The fraction of cells displaying YFP fluorescence depends on the transfection efficiency and the YC-YN interaction. Hence, the percentage of Zinquin accumulation is the fraction of cells accumulating Zinquin solely in cells displaying YFP (*i.e.* YC-YN) fluorescence. Using this dual BiFC-Zinquin assay, we found that co-transfection of *ZnT2-YC-YN* resulted in a significantly higher Zinquin accumulation when compared with transfection of *ZnT1-YC-YN* or *ZnT4-YC-YN* (Fig. 7*A*). This finding is not surprising when considering the role of ZnT1 as a zinc efflux transporter. However, it was unexpected for ZnT4, for which the vesicular localization was similar to that of ZnT2. We suggest that the unique ability of ZnT2 to accumulate Zinquin in vesicles is due to its role in zinc accumulation in vesicles in mammary gland cells during lactation, although further studies are warranted to explore this open question.

We next assessed the functionality of heterodimers formed between ZnT2 and ZnT1 as well as ZnT2 and ZnT4, as reflected in the intravesicular accumulation of Zinquin. As shown in Fig. 1*A*, heterodimers are formed in ~30% of the cells, and with the Zinquin assay, we were able to determine Zinquin accumulation only in cells in which heterodimers formed. Consistent with the PM localization of ZnT1-ZnT2 heterodimers (Fig. 3*m*), we found that when cells were co-transfected with *ZnT1* and *ZnT2* in both configurations of the YC-YN tags, no further increase in Zinquin accumulation was observed (Fig. 7*A*). However, upon co-transfection with YC-YN-tagged *ZnT2* together with *ZnT4*, cells displaying YFP fluorescence due to heterodimerization accumulated marked Zinquin fluorescence levels, hence being comparable with the high fluorescence levels observed with ZnT2-YC-YN homodimers (Fig. 7*A*). It should be noted that the latter occurred despite the fact that at heterodimer transfections, only half of the total amount of plasmid DNA amount was attributable to constructs harboring ZnT2. Although the Zinquin fluorescence of cells expressing ZnT2-ZnT4 heterodimers was not significantly high as were the fluorescence levels of ZnT2 homodimers, ZnT2-ZnT4 heterodimers clearly displayed higher Zinquin fluorescence relative to ZnT1-ZnT2 heterodimers (Fig. 7*A*). These results suggest a zinc transport function for ZnT2-ZnT4 heterodimers, which displayed a Zinquin accumulation that was comparable with that of ZnT2 homodimers. These findings suggest that ZnT2-ZnT4 heterodimers concentrate zinc into intracellular vesicles. Thus, ZnT4 did not interfere with the ability of ZnT2 to concentrate zinc in intracellular vesicles. In contrast, cells harboring ZnT1-ZnT2 heterodimers failed to accumulate Zinquin in intracellular vesicles, due to the drastically altered localization of ZnT2 from intracellular vesicles to the PM, upon formation of ZnT1-ZnT2 heterodimers (Fig. 3*m*).

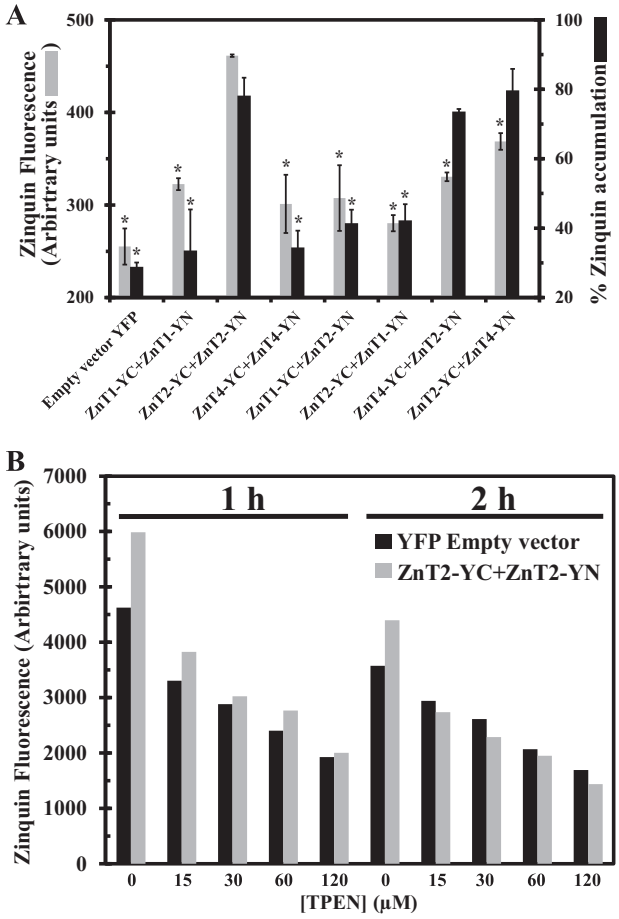

FIGURE 7. **Cellular Zinquin accumulation in ZnT transfectants indicates a zinc transport function for ZnT2-ZnT4 heterodimers.** *A*, MCF-7 cells co-transfected with the constructs depicted along the *x* axis were examined for the percentage of transfected cells displaying Zinquin fluorescence (*gray bars*) as well as Zinquin accumulation levels (*dark bars*). The percentage of transfected cells displaying Zinquin fluorescence was calculated by dividing the fraction of YFP fluorescent cells (YC-YN or YFP) displaying Zinquin fluorescence by the total fraction of cells displaying YFP fluorescence (YC-YN or YFP). *Asterisks* indicate that the values obtained are significantly different ($p < 0.05$) when compared with ZnT2-YC-YN. *Error bars*, S.D. *B*, MCF-7 cells co-transfected with YFP empty vector (*dark bars*) or ZnT2-YC + ZnT2-YN (*gray bars*). The mean Zinquin fluorescence level was determined in the transfected cells in the presence of increasing concentrations (0–120 μM) of TPEN for 1–2 h. A representative experiment is shown.

In order to verify that the Zinquin fluorescence that we observed is due to cellular zinc accumulation, we used increasing concentrations of the cell-permeant zinc chelator TPEN. We found a dose-dependent and time-dependent decrease in Zinquin fluorescence levels when increasing the concentrations of TPEN (0–120 μM) upon 1–2 h of incubation (Fig. 7*B*). These results suggest that the percentage of Zinquin-accumulating cells and the Zinquin fluorescence levels are strictly dependent on zinc accumulation, as revealed by the decrease in Zinquin fluorescence upon TPEN-dependent zinc chelation (Fig. 7*B*).

The G87R Mutation Inflicts a Dominant Negative Effect on Various ZnTs—We have previously shown that the G87R-ZnT2 mutant display a dominant negative effect on the WT ZnT2, as reflected in the ER retention of homodimers of G87R-ZnT2 and WT ZnT2 (11). We therefore evaluated the impact of the G87R-ZnT2 mutant on the subcellular localization of ZnT1, ZnT3, and ZnT4 using the BiFC assay. MCF-7 cells were co-transfected with *ZnT2-YN*, *ZnT3-YN*, or *ZnT4-YN* along with WT *ZnT2-YC* (Fig. 8*A*) or mutant G87R-*ZnT2-YC* (Fig. 8*B*). Co-transfection of the mutant G87R-*ZnT2-YN* along with either *ZnT1-YN*, *ZnT2-YN*, *ZnT3-YN*, or *ZnT4-YN* altered the subcellular localization of heterodimers of both ZnT2-ZnT3 and ZnT2-ZnT4 from intracellular vesicles to the ER network (Fig. 8, *A* and *B*, *g–l*) and of ZnT1-ZnT2 heterodimers from the PM to the ER (Fig. 8, *A* and *B*, *a–c*). These results indicate that the mutant G87R-ZnT2 that causes transient neonatal zinc deficiency inflicts a dominant negative effect not only on homodimers of WT ZnT2 (Fig. 8, *A* and *B*, *d–f*) but also on the localization of ZnT2-ZnT1, ZnT2-ZnT3, and ZnT2-ZnT4 heterodimers. Importantly, heterodimers of ZnT2-YC and ZnT1-YN were localized at the PM (Fig. 8*A*, *a–c*) and showed very low levels of Zinquin accumulation (Fig. 8*A*, *b*). Unsurprisingly, heterodimers of G87R-ZnT2-YC with ZnT1 showed no Zinquin fluorescent vesicles (Fig. 8*B*, *b*). In contrast, heterodimers of ZnT2-ZnT3 and ZnT2-ZnT4 as well as homodimers of WT-ZnT2 showed a high number of Zinquin fluorescent vesicles (Fig. 8*A*, *h* and *k*; note the *blue dots* outside the nucleus), with partial co-localization with the transporters in intracellular vesicles. Replacement of WT-ZnT2 with G87R-ZnT2 resulted in depletion of Zinquin fluorescent vesicles in addition to the dramatic alteration in the subcellular localization (Fig. 8*B*, *d–l*). In order to rule out the possibility that the transfection of this mutant G87R-*ZnT2* that is retained in the ER is due to misfolding and that exposure of a positively charged amino acid in a transmembrane domain leads to an ER stress and to the consequent retention of many membrane proteins at the ER, we determined the levels of the ER stress marker GRP78 (31). GRP78 was used here to determine whether or not an ER stress response is induced in cells transfected with the mutant G87R-*ZnT2*. No significant changes were observed in GRP78 levels when cells were co-transfected with the mutant G87R-*ZnT2* along with the WT-*ZnT2* or with *ZnT4-YC* and *ZnT2-YN* (Fig. 8*C*). These results demonstrate the dominant effect that the mutant G87R-ZnT2 has not only on the WT-ZnT2 via homodimerization but also on ZnT1, ZnT3, and ZnT4 via heterodimerization. Importantly, these results consistently indicate the possible function of heterodimers of ZnT2-ZnT3 as well as ZnT2-ZnT4, as revealed by their vesicular Zinquin accumulation.

Competition on ZnT-YC-YN Dimerization with Non-fluorescent Tagged ZnTs Results in Markedly Decreased Dimer Formation—To provide further evidence that the YFP signal observed upon heterodimerization of ZnT2-YC and ZnT3-YN is due to a specific interaction between these ZnTs and not due to an interaction between the YC-YN tags and their refolding, we undertook a transfection competition assay with non-tagged ZnT cDNAs. We co-transfected MCF-7 cells with equal amounts of expression plasmids harboring YC-YN-tagged ZnTs along with increasing amounts of the competitor plasmid containing the cDNA of non-YC-YN-tagged *ZnT*s (0–2 μg of plasmid DNA) harboring an epitope tag (HA tag for ZnT2 and Myc tag for ZnT3, ZnT5, and the thiamine transporter 1 (THTR1)). We first determined the impact of increasing the amounts of the competitor plasmid harboring *ZnT2-HA* on the

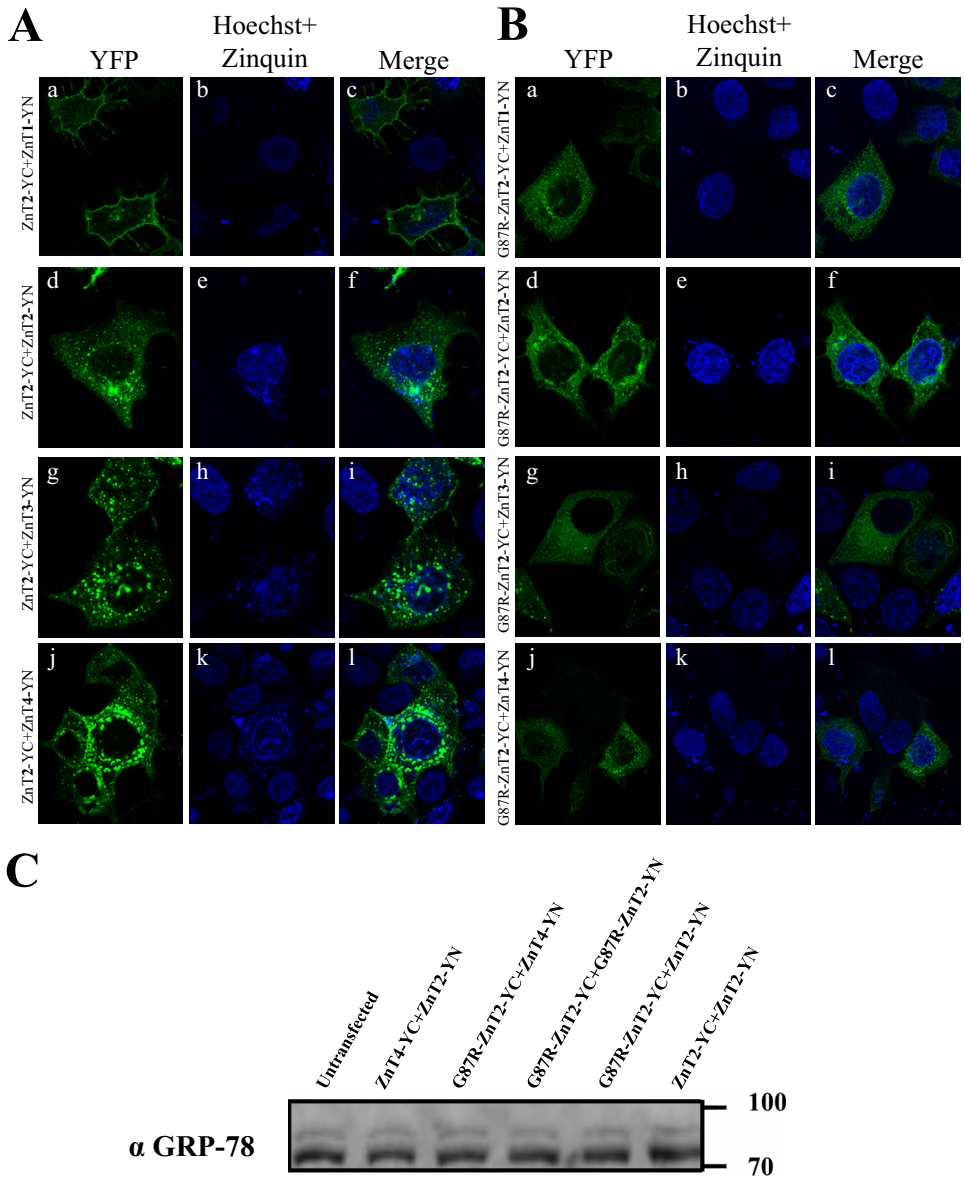

FIGURE 8. **Characterization of mutant heterodimers of G87R ZnT2 and ZnT3 as well as G87R ZnT2 and ZnT4 using BiFC analysis.** MCF-7 cells were transiently co-transfected with WT (*A*) and mutant (*B*) ZnT2 and examined for dimer formation. WT-ZnT2-YC (*A*) or G87R-ZnT2-YC (*B*) was co-transfected along with the vectors depicted on the *left*. YFP fluorescence (*green* fluorescence) indicates homo- or heterodimer formation. Hoechst 33342 (*blue* fluorescence) was used to stain nuclei, and Zinquin (small intracellular vesicles; *blue* fluorescence) was used for zinc staining. *C*, MCF-7 cells were transiently co-transfected with equal amounts of expression plasmids, as depicted *above*. Western blot analysis was performed after SDS-PAGE under denaturing conditions, using an anti-GRP-78 antibody to explore possible ER stress.

formation of ZnT2-YC-YN homodimers (Fig. 9*A*). We observed a dose-dependent decrease in YFP fluorescence when increasing the amounts of the competitor *ZnT2-HA*. The addition of *ZnT2-HA* plasmid DNA at an amount equal to that of *ZnT2-YC* or *ZnT2-YN* (0.5 μg) resulted in a marked decrease in YFP fluorescence levels, and the addition of higher amounts of competitor plasmid DNA further decreased the fluorescence levels. When 2 μg of *ZnT2-HA* plasmid DNA were added, the fluorescence intensity decreased by more than 25% relative to the fluorescence of cells that were transfected solely with *ZnT2-YC-YN* (Fig. 9*A*). We then evaluated the effect of the addition of the *ZnT3-Myc* competitor on ZnT3-YC-YN homodimerization. We consistently observed a significant decrease in the YFP fluorescence in a dose-dependent manner as the amount of *ZnT3-Myc* plasmid DNA was increased. The decrease in the fluorescence intensity of the cells that were co-transfected with *ZnT3-YC* and *ZnT3-YN* along with 2 μg of *ZnT3-Myc* was the most drastic because the fluorescence levels dropped by more than 60% when compared with cells that were not transfected with *ZnT3-Myc* (Fig. 9*B*). We also evaluated the impact of increased amounts of *ZnT2-HA* or *ZnT3-Myc* on the formation of ZnT2-YC-ZnT3-YN heterodimers in order to confirm that the YFP signal observed was due to a specific interaction between ZnT2 and ZnT3. Using *ZnT2-HA* as a competitor for ZnT2-ZnT3 heterodimerization, we observed a significant decrease in the YFP fluorescence in a dose-dependent manner when 1 or 2 μg of the competitor plasmid DNA were added, relative to the initial YFP fluorescence. The addition of 0.5 μg of *ZnT2-HA* plasmid DNA was not sufficient to decrease the YFP fluorescence levels due to the YC-YN refolding (Fig. 9*C*). When

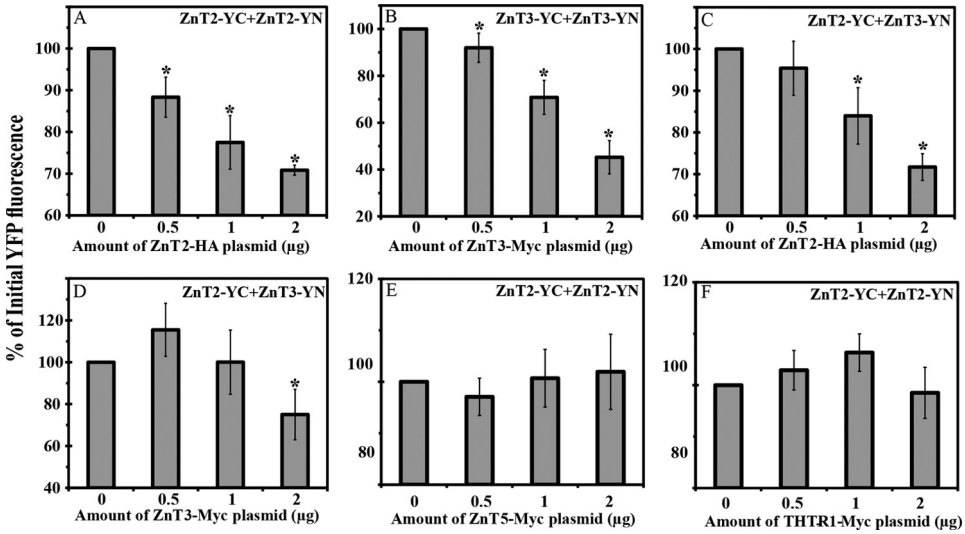

FIGURE 9. **Competition assay with non-YC-YN-tagged ZnT cDNA transfection.** We examined the impact of co-transfection of increasing amounts of competitor ZnT cDNAs along with a constant amount of YC-YN plasmids. MCF-7 cells were transiently co-transfected with an equal amount (total 1 μg from YC-YN DNA plasmids) of ZnT2-YC-YN (*A*, *E*, and *F*), ZnT3-YC-YN (*B*), or ZnT2-YC + ZnT3-YN (*C* and *D*). In addition, cells were co-transfected with increasing amounts of competitor expression plasmids harboring ZnT2-HA (*A* and *C*) or ZnT3-Myc (*B* and *D*), ZnT5-Myc (*E*), and THTR1-Myc (*F*), as described along the *x* axis (0–2 μg of plasmid DNA). Values are presented as the percentage of the mean YFP fluorescence intensity as determined by flow cytometry, when no competitor plasmid was added, which represents the 100% YC-YN fluorescence. *Asterisks* indicate that the values obtained upon competition were significantly different ($p < 0.05$) from the initial (100%) fluorescence levels. *Error bars*, S.D.

ZnT3-Myc was used as a competitor cDNA for ZnT2-ZnT3 heterodimer formation, we observed a significant decrease in the YFP fluorescence levels only when 2 μg of the competitor plasmid DNA were added, compared with the initial YFP fluorescence. In contrast to the other competitions that we performed, the addition of 0.5 μg of the *ZnT3-Myc* plasmid DNA to ZnT2-YC-ZnT3-YN heterodimer formation resulted in a modest increase in the YFP fluorescence levels when compared with the initial fluorescence levels, whereas the addition of 1 μg of *ZnT3-Myc* did not change the YFP fluorescence levels of ZnT2-YC-ZnT3-YN heterodimers (Fig. 9*D*). The difference in the values we observed between ZnT2 and ZnT3 suggests a different affinity for the various dimers of these ZnTs. Furthermore, increasing amounts of the *ZnT5-Myc* and *THTR1-Myc* plasmids were used as negative controls (Fig. 9, *E* and *F*); these plasmids did not significantly decrease the fluorescence levels of ZnT2-YC-YN, thus indicating that no specific interaction of ZnT5 or THTR1 occurred with ZnT2. These results indicate that the driving force of the YC-YN refolding that results in YFP fluorescence is the interaction between the core structure of ZnTs and not the refolding of YC-YN.

DISCUSSION

In the current study, we demonstrated for the first time the ability of various ZnTs to form stable heterodimers. Based on multiple complementary analyses shown below, we demonstrate heterodimer formation of ZnT2 with ZnT1 as well as with ZnT3 and ZnT4. We also identified heterodimers of ZnT4-ZnT1, ZnT3-ZnT4, and ZnT1-ZnT3. All of these heterodimers displayed moderate YFP fluorescence levels in a substantial fraction of transfectant cells, when compared with the high YFP fluorescence of their cognate homodimers, but significantly higher than the negative controls. Using the various complementary techniques detailed below, we provide several lines of experimental evidence corroborating the formation of heterodimers in the ZnT family. (*a*) We first performed a wide BiFC screen of multiple ZnTs using flow cytometric analysis following transient co-transfection of multiple YC-YN-tagged *ZnT*s. This sensitive BiFC technique allowed for the initial selection of specific ZnT candidates displaying a relatively strong heterodimerization. (*b*) Fluorescence microscopy was used as a complementary assay for the assessment of the intracellular co-localization of the heterodimers that were identified with the BiFC constructs. (*c*) Prompted by the unique ability of the YC-YN fragments to refold and form covalent bonds, we corroborated the physical interaction between the ZnT monomers that form different heterodimers by Western blot analysis. (*d*) Immunofluorescence microscopy revealed the co-localization of ZnT2 with ZnT3 in intracellular vesicles using HA- and Myc-tagged epitopes, hence further suggesting the interaction between these transporters. (*e*) To rule out the remote possibility that the YC-YN fragment tags were the driving force of ZnT heterodimerization, we undertook a cDNA competition assay with HA- and Myc-tagged *ZnT*s in order to verify that the core protein-protein interaction between various ZnTs is the driving force that leads to the YFP fluorescence observed upon heterodimerization. These complementary techniques proved instrumental in the first demonstration of the existence of multiple ZnT heterodimers. These novel findings shed new light on the ZnT-dependent mechanisms underlying intracellular zinc homeostasis in health and disease.

Previous studies showing homo- or heterodimerization in the ZnT family were based on biochemical assays combined with immunofluorescence microscopy co-localization of individual ZnTs in the same subcellular compartment (11, 20, 21, 32). The most established heterodimer was ZnT5-ZnT6, which was shown to function in the activation of tissue-nonspecific

alkaline phosphatase at this heterodimer form (21). In a previous review, Lazarczyk *et al.* (32) described the ability of ZnT1 to interact with either EVER1/EVER2 proteins, ZnT1–4, or ZnT7, as revealed by a yeast two-hybrid screening assay. However, experimental data that pinpoint these putative interactions and their functionality at their intracellular localization in viable mammalian cells have not been provided. Using the BiFC assay, we found here a drastically altered subcellular localization of various ZnTs upon heterodimerization. ZnTs are known to localize at distinct subcellular compartments, depending on their function as well as their tissue-specific expression pattern (6, 33). ZnT1 is predominantly localized at the PM, and it displays a major role as a zinc exporter that protects cells from zinc toxicity (6, 34). ZnT3 was shown to localize at synaptic vesicles (20), whereas ZnT2 and ZnT4 have been shown to reside in the membrane of intracellular vesicles/granules, including lysosomes and endosomes (6, 26, 35), and in a small fraction of cells in the PM (36). We found a drastically altered subcellular localization of ZnT1-ZnT2 and ZnT1-ZnT4 heterodimers, which surprisingly resided in the PM. Hence, ZnT2 and ZnT4 acquired a completely different localization from their intracellular vesicle localization that is characteristic to their homodimeric state. In contrast, ZnT3-ZnT1 heterodimers localized at intracellular vesicles and were not directed to the PM; therefore, upon heterodimerization with ZnT3, ZnT1 acquired a completely different localization when compared with its PM localization that is characteristic of ZnT1 homodimers. Our results suggest that multiple ZnTs undergo heterodimerization and may acquire a new subcellular localization, thereby creating an intricate network of homodimers and heterodimers that may play a key role in maintenance of zinc homeostasis under physiological and pathological conditions.

In contrast to ZnT5-ZnT6 heterodimers, which largely do not function as homodimers (21), all of the heterodimers that we identified here are known to be active in zinc transport at the homodimer state. This raises a complex question of how to discern experimentally the functions of heterodimers from those of their cognate homodimers. Using the dual BiFC-Zinquin assay that we recently introduced (22), we suggest here that MCF-7 cells transfected with ZnT2 showed high levels of Zinquin vesicular accumulation, although the exact organelles of this accumulation and of ZnT2 are still unclear. We suggest that ZnT2 enhanced the formation of zinc-containing vesicles, termed "zincosomes" (1) in order to reduce cytosolic zinc levels and serve as a zinc buffer. ZnT2-ZnT3 as well as ZnT2-ZnT4 heterodimers preserved this ability of zinc accumulation in vesicles, as indicated by the high number of Zinquin vesicles in cells harboring these heterodimers. On the other hand, ZnT1-ZnT2 heterodimers failed to accumulate Zinquin above the background level. This difference could be easily explained by the fact that ZnT1-ZnT2 heterodimers were localized at the PM and hence presumably functioned as a zinc efflux transporter. Further studies are warranted to address the question of the functionality of endogenous ZnTs upon heterodimer formation.

The BiFC assay was previously applied for the identification of multiple protein-protein interactions and to detect alterations in the intracellular localization and function of various proteins that undergo dimerization. For example, heterodimerization of bZIP and Rel proteins studied by BiFC was shown to affect their subcellular localization and modulated the transcriptional transactivation capacity (23). Likewise, the BiFC assay was employed to corroborate the homodimerization and drug extrusion function of the multidrug resistance efflux transporter ABCG2 (BCRP) (37). Moreover, different C/EBPβ dimers were shown to localize in different nuclear domains using BiFC (38). Hence, the BiFC technique has been recently shown to serve as an excellent tool for the dissection of the pharmacology of G-protein-coupled receptor signaling complexes composed of seven-transmembrane domain G-protein-coupled receptors, G-proteins, and β-arrestins (39). However, while using the BiFC assay, it is important to evaluate the background fluorescence levels of protein pairs that do not specifically interact with each other, which can readily serve as a negative control. In our BiFC experiments, we used the membrane receptor β2AR (40) as a negative control as it does not interact with ZnTs (22). Moreover, competition by interactions with endogenous or untagged proteins is considered to be the major mechanism that determines the specificity of the BiFC complex in living cells (30). In order to verify that the YFP fluorescence signal observed was due to a specific ZnT heterodimerization and not due to a spontaneous refolding of the YC-YN tags, we undertook a competition assay with various non-fluorescent HA- or Myc-tagged *ZnT* cDNAs. Indeed, we observed a dose-dependent decrease in YFP fluorescence when increasing the amounts of the competitor *ZnT2/ZnT3* plasmid. The ability of a specific ZnT to compete on the YC-YN homodimerization or heterodimerization varied between the different ZnTs. These findings are likely to reflect the variable strength of interactions occurring between various ZnTs. While assuming that the expression levels of the competitor vectors were equal, one can infer that the interactions between ZnT3 homodimers are weaker relative to ZnT2 homodimers and thereby were more sensitive to competition with *ZnT* cDNA. In addition, this may be the reason for the lower competition capacity that *ZnT3-Myc* had on ZnT2-ZnT3 heterodimers when compared with *ZnT2-HA* that achieved a dose-dependent decrease in the YFP fluorescence signal. Importantly, the decrease in the YFP fluorescence in a dose-dependent manner upon an increase in the amount of the competitor ZnT plasmid indicated that the driving force for the formation of YFP fluorescence was the physical association between the different ZnT proteins and not the association between the YC and YN tags. Although the ZnT2-YC-ZnT3-YN heterodimer results indicated that these interactions are not the primarily dominant interactions of these transporters, the inherent irreversibility of mature refolded YC-YN can serve as a molecular magnifying glass for these specific interactions between various ZnTs that otherwise could not be easily detected.

Based on the Human Protein Atlas, ZnT2, ZnT3, and ZnT4 are co-expressed in moderate to high levels in human tissues, such as pancreas and testis. ZnT protein levels in different organelles may vary due to different physiologic cues, such as lactation or pregnancy, or due to certain pathologic states. For example, ZnT2 is up-regulated in the mammary gland during lactation through the elevation of prolactin, which acts as a

transcriptional transactivator (41). As an example of a pertaining pathological state, ZnT3 mRNA levels were shown to be markedly reduced in brain tissue from patients with Alzheimer disease (42). Although women carrying the G87R-ZnT2 mutation did not show other known related symptoms except for low levels of zinc in their breast milk (11, 13), based on our current data instigating heterodimerization of ZnT2 with ZnT1, ZnT2 with ZnT3, and ZnT2 with ZnT4, it is possible that the dominant negative effect of the G87R-ZnT2 mutant mediates additional pathologic alterations on other ZnTs that were not described before. Heterodimerization of G87R-ZnT2 with other ZnTs (Fig. 8) drastically altered the subcellular localization of these transporters. Further molecular and clinical examination should be performed to address the question of the possible deleterious effects of different variants/mutants of ZnT2 and their relation to other pathological states. In addition, it will be interesting to evaluate the fertility status of males harboring ZnT2 mutations regarding the functionality of tissues such as testis and prostate which are highly dependent on zinc. Moreover, further experiments should be performed to address the question of the physiologic states that lead to ZnT heterodimer formation, and the different functions of this heterodimers when compared with their cognate homodimers.

In summary, we provided here the first direct visual evidence for the *in situ* heterodimerization and function of various ZnTs in live cells using the BiFC assay and various complementary techniques. The existence of multiple ZnT heterodimers suggests a new insight regarding the underlying molecular and cellular mechanisms that maintain intracellular zinc homeostasis under physiologic conditions and pathologic states. Moreover, the current findings shed a new light on protein-protein interactions that may alter subcellular localization and function of various ZnTs. These novel findings expand our understanding of the intricate and complex network of zinc transporters that may form homo- and heterodimers contributing to the maintenance of zinc homeostasis.

Acknowledgment—We thank Eliran Passand for assistance with some of the BiFC experiments.

REFERENCES

1. Eide, D. J. (2006) Zinc transporters and the cellular trafficking of zinc. *Biochim. Biophys. Acta* **1763,** 711–722
2. Palmiter, R. D., and Huang, L. (2004) Efflux and compartmentalization of zinc by members of the SLC30 family of solute carriers. *Pflugers Arch.* **447,** 744–751
3. Wessells, K. R., and Brown, K. H. (2012) Estimating the global prevalence of zinc deficiency: results based on zinc availability in national food supplies and the prevalence of stunting. *PLoS One* **7,** e50568
4. Prasad, A. S. (2012) Discovery of human zinc deficiency: 50 years later. *J. Trace Elem. Med. Biol.* **26,** 66–69
5. Lee, J., Yim, Y. S., Ko, S. J., Kim, D. G., and Kim, C. H. (2011) Gap junctions contribute to astrocytic resistance against zinc toxicity. *Brain Res. Bull.* **86,** 314–318
6. Huang, L., and Tepaamorndech, S. (2013) The SLC30 family of zinc transporters: a review of current understanding of their biological and pathophysiological roles. *Mol. Aspects Med.* **34,** 548–560
7. Jeong, J., and Eide, D. J. (2013) The SLC39 family of zinc transporters. *Mol. Aspects Med.* **34,** 612–619
8. Chowanadisai, W., Lönnerdal, B., and Kelleher, S. L. (2006) Identification of a mutation in SLC30A2 (ZnT-2) in women with low milk zinc concentration that results in transient neonatal zinc deficiency. *J. Biol. Chem.* **281,** 39699–39707
9. Itsumura, N., Inamo, Y., Okazaki, F., Teranishi, F., Narita, H., Kambe, T., and Kodama, H. (2013) Compound heterozygous mutations in SLC30A2/ZnT2 results in low milk zinc concentrations: a novel mechanism for zinc deficiency in a breast-fed infant. *PLoS One* **8,** e64045
10. Krieger, I., Alpern, B. E., and Cunnane, S. C. (1986) Transient neonatal zinc deficiency. *Am. J. Clin. Nutr.* **43,** 955–958
11. Lasry, I., Seo, Y. A., Ityel, H., Shalva, N., Pode-Shakked, B., Glaser, F., Berman, B., Berezovsky, I., Goncearenco, A., Klar, A., Levy, J., Anikster, Y., Kelleher, S. L., and Assaraf, Y. G. (2012) A dominant negative heterozygous G87R mutation in the zinc transporter, ZnT-2 (SLC30A2), results in transient neonatal zinc deficiency. *J. Biol. Chem.* **287,** 29348–29361
12. Lova Navarro, M., Vera Casaño, A., Benito Lopez, C., Fernández Ballesteros, M. D., Godoy Díaz, D. J., Crespo Erchiga, A., and Romero Brufau, S. (2014) Transient neonatal zinc deficiency due to a new autosomal dominant mutation in gene SLC30A2 (ZnT-2). *Pediatr. Dermatol.* **31,** 251–252
13. Miletta, M. C., Bieri, A., Kernland, K., Schöni, M. H., Petkovic, V., Flück, C. E., Eblé, A., and Mullis, P. E. (2013) Transient neonatal zinc deficiency caused by a heterozygous G87R mutation in the zinc transporter ZnT-2 (SLC30A2) gene in the mother highlighting the importance of Zn^{2+} for normal growth and development. *Int. J. Endocrinol.* **2013,** 259189
14. Adlard, P. A., Parncutt, J. M., Finkelstein, D. I., and Bush, A. I. (2010) Cognitive loss in zinc transporter-3 knock-out mice: a phenocopy for the synaptic and memory deficits of Alzheimer's disease? *J. Neurosci.* **30,** 1631–1636
15. Weijers, R. N. (2010) Three-dimensional structure of β-cell-specific zinc transporter, ZnT-8, predicted from the type 2 diabetes-associated gene variant SLC30A8 R325W. *Diabetol Metab. Syndr.* **2,** 33
16. Gohlke, H., Ferrari, U., Koczwara, K., Bonifacio, E., Illig, T., and Ziegler, A. G. (2008) SLC30A8 (ZnT8) Polymorphism is associated with young age at type 1 diabetes onset. *Rev. Diabet. Stud.* **5,** 25–27
17. Coudray, N., Valvo, S., Hu, M., Lasala, R., Kim, C., Vink, M., Zhou, M., Provasi, D., Filizola, M., Tao, J., Fang, J., Penczek, P. A., Ubarretxena-Belandia, I., and Stokes, D. L. (2013) Inward-facing conformation of the zinc transporter YiiP revealed by cryoelectron microscopy. *Proc. Natl. Acad. Sci. U.S.A.* **110,** 2140–2145
18. Lu, M., and Fu, D. (2007) Structure of the zinc transporter YiiP. *Science* **317,** 1746–1748
19. Lu, M., Chai, J., and Fu, D. (2009) Structural basis for autoregulation of the zinc transporter YiiP. *Nat. Struct. Mol. Biol.* **16,** 1063–1067
20. Salazar, G., Falcon-Perez, J. M., Harrison, R., and Faundez, V. (2009) SLC30A3 (ZnT3) oligomerization by dityrosine bonds regulates its subcellular localization and metal transport capacity. *PLoS One* **4,** e5896
21. Fukunaka, A., Suzuki, T., Kurokawa, Y., Yamazaki, T., Fujiwara, N., Ishihara, K., Migaki, H., Okumura, K., Masuda, S., Yamaguchi-Iwai, Y., Nagao, M., and Kambe, T. (2009) Demonstration and characterization of the heterodimerization of ZnT5 and ZnT6 in the early secretory pathway. *J. Biol. Chem.* **284,** 30798–30806
22. Lasry, I., Golan, Y., Berman, B., Amram, N., Glaser, F., and Assaraf, Y. G. (2014) *In situ* dimerization of multiple wild type and mutant zinc transporters in live cells using bimolecular fluorescence complementation. *J. Biol. Chem.* **289,** 7275–7292
23. Hu, C. D., Chinenov, Y., and Kerppola, T. K. (2002) Visualization of interactions among bZIP and Rel family proteins in living cells using bimolecular fluorescence complementation. *Mol. Cell* **9,** 789–798
24. Kerppola, T. K. (2006) Design and implementation of bimolecular fluorescence complementation (BiFC) assays for the visualization of protein interactions in living cells. *Nat. Protoc.* **1,** 1278–1286
25. Falcón-Pérez, J. M., and Dell'Angelica, E. C. (2007) Zinc transporter 2 (SLC30A2) can suppress the vesicular zinc defect of adaptor protein 3-depleted fibroblasts by promoting zinc accumulation in lysosomes. *Exp. Cell Res.* **313,** 1473–1483
26. Kukic, I., Kelleher, S. L., and Kiselyov, K. (2014) Zinc efflux through lysosomal exocytosis prevents zinc-induced toxicity. *J. Cell Sci.* **127,** 3094–3103

27. Seo, Y. A., and Kelleher, S. L. (2010) Functional analysis of two single nucleotide polymorphisms in SLC30A2 (ZnT2): implications for mammary gland function and breast disease in women. *Physiol. Genomics* **42A,** 219–227
28. Lopez, V., and Kelleher, S. L. (2009) Zinc transporter-2 (ZnT2) variants are localized to distinct subcellular compartments and functionally transport zinc. *Biochem. J.* **422,** 43–52
29. Seo, Y. A., Lopez, V., and Kelleher, S. L. (2011) A histidine-rich motif mediates mitochondrial localization of ZnT2 to modulate mitochondrial function. *Am. J. Physiol. Cell Physiol.* **300,** C1479–C1489
30. Kerppola, T. K. (2009) Visualization of molecular interactions using bimolecular fluorescence complementation analysis: characteristics of protein fragment complementation. *Chem. Soc. Rev.* **38,** 2876–2886
31. Lee, A. S. (2005) The ER chaperone and signaling regulator GRP78/BiP as a monitor of endoplasmic reticulum stress. *Methods* **35,** 373–381
32. Lazarczyk, M., Cassonnet, P., Pons, C., Jacob, Y., and Favre, M. (2009) The EVER proteins as a natural barrier against papillomaviruses: a new insight into the pathogenesis of human papillomavirus infections. *Microbiol. Mol. Biol. Rev.* **73,** 348–370
33. Kambe, T., Hashimoto, A., and Fujimoto, S. (2014) Current understanding of ZIP and ZnT zinc transporters in human health and diseases. *Cell. Mol. Life Sci.* **71,** 3281–3295
34. Nolte, C., Gore, A., Sekler, I., Kresse, W., Hershfinkel, M., Hoffmann, A., Kettenmann, H., and Moran, A. (2004) ZnT-1 expression in astroglial cells protects against zinc toxicity and slows the accumulation of intracellular zinc. *Glia* **48,** 145–155
35. Michalczyk, A. A., Allen, J., Blomeley, R. C., and Ackland, M. L. (2002) Constitutive expression of hZnT4 zinc transporter in human breast epithelial cells. *Biochem. J.* **364,** 105–113
36. Overbeck, S., Uciechowski, P., Ackland, M. L., Ford, D., and Rink, L. (2008) Intracellular zinc homeostasis in leukocyte subsets is regulated by different expression of zinc exporters ZnT-1 to ZnT-9. *J. Leukoc. Biol.* **83,** 368–380
37. Haider, A. J., Briggs, D., Self, T. J., Chilvers, H. L., Holliday, N. D., and Kerr, I. D. (2011) Dimerization of ABCG2 analysed by bimolecular fluorescence complementation. *PLoS One* **6,** e25818
38. Susperreguy, S., Prendes, L. P., Desbats, M. A., Charó, N. L., Brown, K., MacDougald, O. A., Kerppola, T., Schwartz, J., and Piwien-Pilipuk, G. (2011) Visualization by BiFC of different C/EBPβ dimers and their interaction with HP1α reveals a differential subnuclear distribution of complexes in living cells. *Exp. Cell Res.* **317,** 706–723
39. Kilpatrick, L. E., and Holliday, N. D. (2012) Dissecting the pharmacology of G protein-coupled receptor signaling complexes using bimolecular fluorescence complementation. *Methods Mol. Biol.* **897,** 109–138
40. Vaniotis, G., Allen, B. G., and Hébert, T. E. (2011) Nuclear GPCRs in cardiomyocytes: an insider's view of β-adrenergic receptor signaling. *Am. J. Physiol. Heart Circ. Physiol.* **301,** H1754–H1764
41. Qian, L., Lopez, V., Seo, Y. A., and Kelleher, S. L. (2009) Prolactin regulates ZNT2 expression through the JAK2/STAT5 signaling pathway in mammary cells. *Am. J. Physiol. Cell Physiol.* **297,** C369–C377
42. Beyer, N., Coulson, D. T., Heggarty, S., Ravid, R., Irvine, G. B., Hellemans, J., and Johnston, J. A. (2009) ZnT3 mRNA levels are reduced in Alzheimer's disease post-mortem brain. *Mol. Neurodegener.* **4,** 53